PHILOSOPHICAL TRANSACTIONS OF THE ROYAL SOCIETY A MATHEMATICAL, PHYSICAL & ENGINEERING SCIENCES

Bioturbation and Manganese Cycling in Hemipelagic Sediments

R. C. Aller

Phil. Trans. R. Soc. Lond. A 1990 **331**, 51-68
doi: 10.1098/rsta.1990.0056

Phil. Trans. R. Soc. Lond. A **331**, 51–68 (1990) [51]
Printed in Great Britain

Bioturbation and manganese cycling in hemipelagic sediments

By R. C. Aller

Marine Sciences Research Center, State University of New York, Stony Brook, New York 11794-5000, *U.S.A.*

The activities of infaunal macrobenthos have major influences on the types, rates and distributions of diagenetic reactions involving manganese in relatively carbon-rich deep-sea and nearshore sediments. In some non-sulphidic hemipelagic deposits of the eastern equatorial Pacific (Panama Basin) biogenic reworking drives internal cycles of manganese, which can apparently account for up to *ca.* 100% of organic carbon oxidation and reduction of O_2 supplied (diffusively) to the sea floor. Heterotrophic (carbon-based) manganese reduction is stimulated by simultaneous mixing of reactive organic matter and manganese oxide into suboxic–anoxic deposits. In sulphidic sediments, biogenic reworking must also enhance a lithotrophic pathway (sulphur-based) pathway of manganese reduction by promoting contact of manganese oxides and iron sulphides. Particle reworking dramatically alters the balance between aerobic and anaerobic decomposition pathways, promoting the utilization of O_2 in the reoxidaton of reduced metabolites rather than direct oxidation of carbon. Irrigated burrows create microenvironments, which increase manganese reduction–oxidation and deplete Mn^{2+} from deeper pore waters. This may increase net Mn^{2+} production rates by removal of metabolites and potential co-precipitants with Mn^{2+}. The occurrence and geometry of manganese oxide encrusted biogenic structures imply specific adaptations of infauna to manganese based microbial activity in hemipelagic sediments like the Panama Basin.

Introduction

In most sedimentary deposits underlying oxygenated waters, the activities of macrobenthic organisms have significant effects on diagenetic reactions, sediment–water exchange and the composition of sediments eventually preserved. Feeding, burrowing, tube construction and burrow irrigation by macrobenthos result in particle and fluid transport. These transport processes influence reaction distributions, solute diffusion geometries and the relative and absolute rates of reactions in a deposit. Such effects can be particularly significant in organic carbon-rich sediments typical of hemipelagic and nearshore regions. Here I discuss in particular how macrobenthos interact with manganese cycling during early diagenesis and how organic matter decomposition reaction balances and rates are affected by particle reworking and burrow irrigation in hemipelagic sediments.

It is commonly emphasized that aerobic (O_2) metabolism dominates the decomposition of organic matter in deep-sea sediments and that anaerobic pathways (oxidants are NO_3, MnO_2, FeOOH, SO_4) are of relatively minor importance (Jahnke *et al.* 1982; Bender & Heggie 1984; Emerson *et al.* 1985). In contrast, anaerobic decomposition, particularly sulphate reduction, often dominates in shallow water organic-rich deposits, where much of the oxygen flux to the sea bed reoxidizes reduced products of anaerobic decomposition such as NH_4^+, HS^- and Fe sulphides rather than oxidizing carbon directly (Jorgensen 1982; Chanton *et al.* 1987; Mackin

& Swider 1989). Hemipelagic sediments typically represent an intermediate class of deep-water environments in which the organic carbon flux to the sea floor is sufficiently large that oxygen is depleted within a few centimetres of the sediment–water interface (Reimers 1987), but not so great as to result in sulphidic deposits. It seems likely that in such regions, sedimentary redox reaction balances must generally lie between the extremes of the oligothropic deep-water regions (Grundmanis & Murray 1982) and the sulphidic–methanogenic nearshore.

In at least one large hemipelagic region, the east equatorial Pacific, oceanographic conditions favouring upwelling and high primary production come together with tectonic conditions favouring hydrothermal production (Boström & Peterson 1969; Manheim & Lane-Bostwick 1989; Moore *et al.* 1973; Honjo 1982). This causes the delivery of relatively large amounts of both biogenic reactive organic carbon and hydrothermal manganese to the sea floor (figure 1). The result is an active, deep-water benthic community that promotes and interacts with suboxic diagenetic reactions, particularly the manganese cycle.

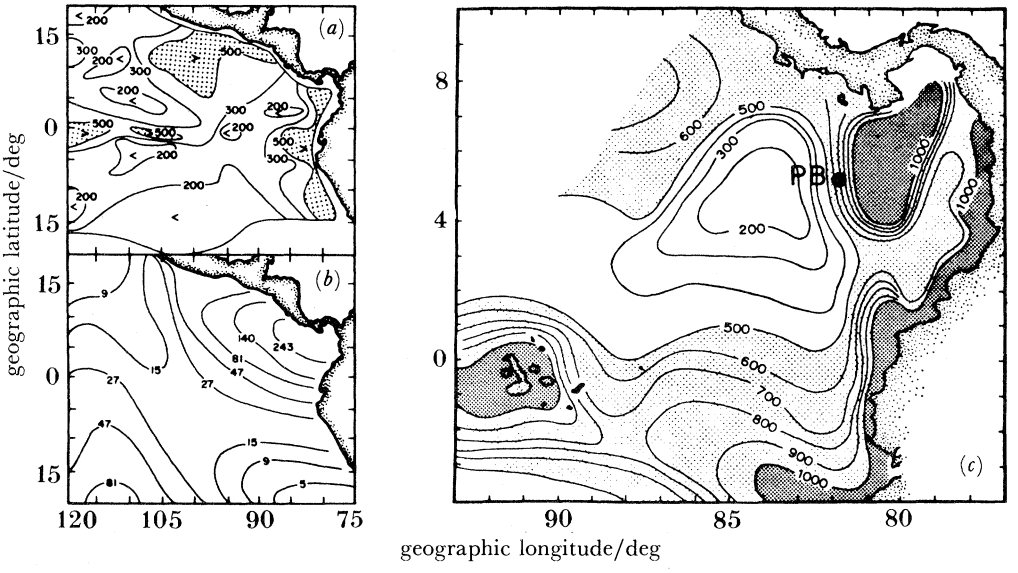

FIGURE 1. Oceanographic and tectonic conditions accentuate both carbon and manganese delivery to the sea floor in the east equatorial Pacific. (*a*) Primary production, pattern, February–March; (after Love & Allen 1975; Lyle 1983). (*b*) Manganese crust estimated accumulation rates, (mm Ma^{-1}), (after Manheim & Lane-Bostwick 1988). (*c*) Mean annual primary production (euphotic zone, mg m^{-2} d^{-1}) (Moore *et al.* 1973) and station PB location in Panama Basin.

Example: the Panama Basin

A single, relatively well-studied site in the Panama Basin (PB) of the east equatorial Pacific will be used here to illustrate both the diagenetic properties of the sediments in this general region and basic interactions between different processes in the bioturbated zone of hemipelagic muds. The PB station is located at 5° 20.65′ N, 81° 56.19′ W in a deep depression (3890 m) between the Coiba and Malpelo Ridges (figure 1*c*). Bottom-water potential temperature, salinity and oxygen are *ca.* 1.8 °C, 34.67‰ and *ca.* 110 μM respectively (Laird 1971; Lonsdale 1976; Spencer 1979). General current flow (less than a few cm s^{-1}) is east to west in the region and no nonepheloid layer is detectable (Laird 1971; Lonsdale 1976; Honjo *et al.* 1982).

Primary production in Panama Basin overlying waters shows high east–west spatial gradients between 500 and 1000 mg m^{-2} d^{-1} in this region and is seasonally variable with highest production in February–March and June–July (Moore *et al.* 1973; Honjo 1982). Bottom muds generally contain *ca.* 30 % biogenic material ($CaCO_3$, SiO_2) (Heath *et al.* 1974) and, at the site examined here, have 2–3 % organic carbon, 15–20 % $CaCO_3$ and 7–11 % biogenic SiO_2 in about the upper 25 cm (Mackin & Aller 1984). The clay fraction is predominantly smectite (50–70 %) with chlorite (15–20 %), illite (5–10 %) and kaolinite (10–15 %) (Heath *et al.* 1983).

The average annual flux of organic carbon to the bottom area is *ca.* 40 μmol cm^{-2} a^{-1} and much of this is apparently relatively unaltered planktonic debris arriving in major pulses (Honjo 1982; Cole *et al.* 1985). An abundant macroinfauna (*ca.* 1900–2300 individuals per square metre), numerically dominated by polychaetes and tanaids (R. Whitlatch & J. Grassle, personal communication), rapidly reworks bottom sediments to depths greater than 30 cm. During at least some periods, excess ^{234}Th (24-day half-life) is mixed to several centimetres, yielding particle mixing coefficients of *ca.* 20–30 cm^2 a^{-1} comparable with shallow water, nearshore environments (Aller & DeMaster 1984). Excess ^{210}Pb distributions (22-year half-life) are essentially homogeneous in the upper 6–8 cm and demonstrate a more slowly mixed zone (*ca.* 1 cm^2 a^{-1}) at depths of approximately 10–30 cm (figure 2; Aller & DeMaster 1984). *In situ* mixing experiments with stable glass bead tracers also show rapid penetration of particles near the interface, but at rates 2–3 times lower than those estimated from ^{234}Th (R. Whitlatch & J. Grassle, personal communication).

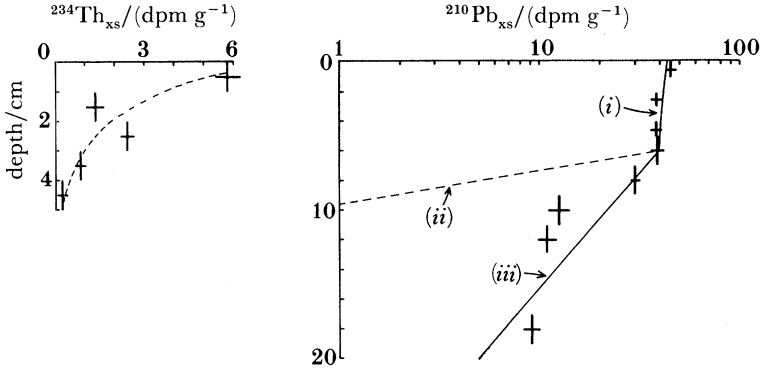

FIGURE 2. Excess ^{234}Th and ^{210}Pb profiles demonstrate particle reworking rates greater than or equal to 10 cm^2 a^{-1} in about the upper 6 cm and greater than or equal to 1 cm^2 a^{-1} to depths of 24–30 cm (after Aller & DeMaster 1984). (i) D_B (1) = 23 cm^2 a^{-1}, (ii) $D_B(2) = 0$, (iii) $D_B(2) = 1.2$ cm^2 a^{-1}.

As a result of relatively intense macrofaunal activity, deposits are dominated by biogenic rather than physically formed structures. Networks of small burrows (*ca.* 1 mm in diameter) are interspersed with larger tubes or burrows of varied size and type. Evidence of large, mobile infauna and epifauna is present as both abundant tracks and trails at the surface (snails) and internal structures (characteristic of heart urchins). Echiurid burrows and surface feeding traces are common, as are relict burrows infilled almost exclusively with well-formed fecal pellets (*ca.* 0.5 mm diameter).

Pore water profiles at PB of solutes produced or consumed during organic matter decomposition show patterns typical of suboxic diagenesis (figure 3; Froelich *et al.* 1979).

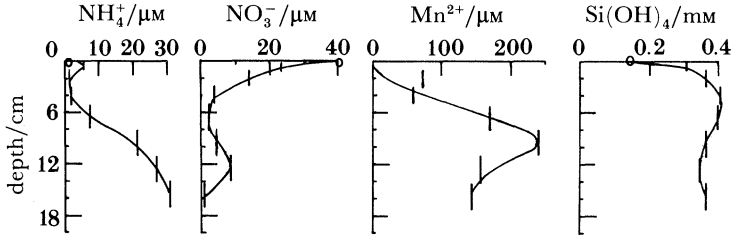

FIGURE 3. Representative pore water solute patterns in surface processed cores from station PB. Oxygen is absent below *ca.* (0.8 ± 0.3) cm depth, except around burrow structures.

Oxygen penetrates approximately (0.8 ± 0.3) cm on the average below the upper sediment water interface, as measured on retrieved cores using microelectrodes (Cole *et al.* 1987; Aller *et al.* 1987). Deeper penetration occurs radially around irrigated burrow structures. The basic patterns demonstrated in tens of retrieved cores (processed at 2 °C) are: depletion of NO_3^- by 6–10 cm underlain by secondary maxima from 10–16 cm; surface (0–1 cm maxima of NH_4^+ followed by regular build-up below 3–4 cm; concave upward increases of Mn^{2+} below 2–3 cm to 150–350 μM by *ca.* 8–16 cm; regular increases in alkalinity to 3–3.5 meg dm^{-3} at 6–12 cm; and increases in $Si(OH)_4$ to *ca.* 400 μM by 2–3 cm with depletion at depth. These patterns are also generally found in *in situ* pore water equilibration probes, although some features such as the interface NH_4^+ peak, are absent and are apparently artefacts produced by core retrieval (Aller *et al.* 1987). Other solute gradients (e.g. NO_3^-) near the interface may also be slight overestimates in retrieved cores due to decompression and warming during recovery. The major observation is that NO_3^- reduction and manganese reduction dominate oxidation–reduction reactions below 0–1 cm. No evidence of Fe or SO_4 reduction is found in pore water profiles in the upper 25 cm.

The overall idealized reactions likely to influence the observed pore water solute distributions are listed in table 1. Oxygen is consumed by carbon, NH_4^+ and Mn^{2+} oxidation. NO_3^- and manganese oxide reduction apparently take place simultaneously in these sediments. At least a portion of the NO_3^- could theoretically oxidize Mn^{2+} at the observed solute concentrations and pH (7.6–7.9). Such a reaction is consistent with concave-upward distributions in Mn^{2+} below the oxygenated zone but has not been directly demonstrated. NO_3^- can theoretically also

TABLE 1. IDEALIZED REACTIONS LIKELY TO INFLUENCE THE OBSERVED PORE WATER SOLUTE DISTRIBUTIONS

oxygen reduction

$$C_{org} + O_2 \rightarrow CO_2,$$
$$NH_3 + O_2 \rightarrow NO_3^- + H_2O + H^+,$$
$$Mn^{2+} + \tfrac{1}{2}O_2 + H_2O \rightarrow MnO_2 + 2H^+.$$

nitrate reduction–denitrification

$$2H_2O + 5C_{org} + 4NO_3^- \rightarrow 4HCO_3 + 2N_2 + CO_2,$$
$$4H_2O + 5Mn^{2+} + 2NO_3^- \rightarrow 5MnO_2 + N_2 + 8H^+,$$
$$2OH^- + 5NH_4^+ + 3NO_3^- \rightarrow 4N_2 + 11H_2O.$$

manganese reduction

$$C_{org} + 2MnO_2 + 3CO_2 + 2H_2O \rightarrow 4HCO_3^- + 2Mn^{2+}.$$

manganese carbonate precipitation

$$x Mn^{2+} + (1-x)\,Ca^{2+} + 2HCO_3^- \rightarrow Mn_x\,Ca_{1-x}\,CO_3 + CO_2 + H_2O.$$

oxidize NH_4^+ to N_2 (Bender *et al.* 1989). The eventual decrease in Mn^{2+} with depth presumably reflects precipitation of proto-kutnahorite-like manganese carbonate phases known to occur in these deposits (Petersen & Price 1982).

The upward flux of Mn^{2+} and its reoxidation result in the enrichment of solid phase manganese in surface sediments of the Panama Basin site (figure 4). These surface enrichments are regionally common (Boström & Pederson 1969; Petersen & Price 1982), reflecting hydrothermal sources and the widely recognized process of manganese recycling during oxic–suboxic diagenesis. The magnitude and the large depth gradients of manganese enrichment imply a substantial role for manganese in oxidation–reduction reactions in these deposits.

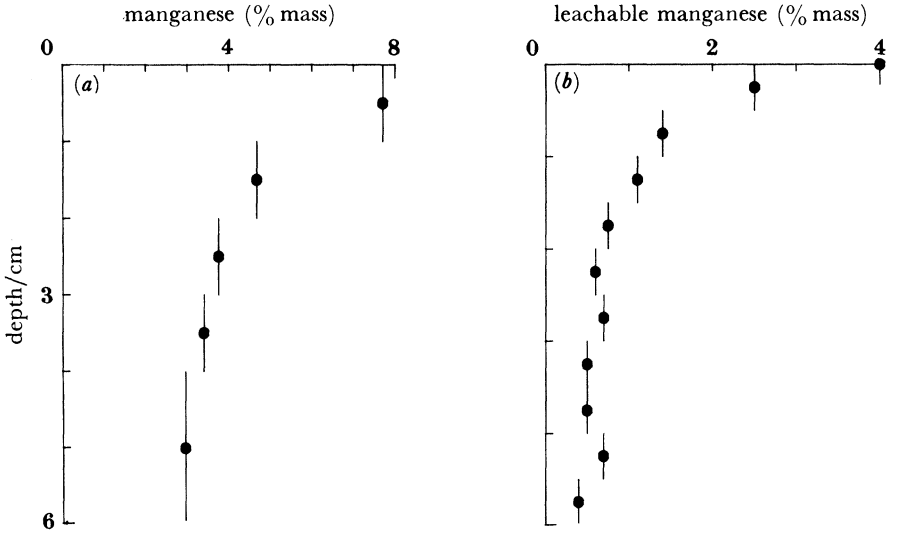

FIGURE 4. Manganese is dramatically enriched in the upper few centimetres at PB. (*a*) Example of 6N HCl leachable manganese (total) distribution. (*b*) 'Manganese-oxyhydroxide' distribution (acetic acid/hydroxylamine leachable, after Balistrieri & Murray (1986)).

Manganese reduction rates

The rate of manganese reduction can be estimated from both the solid phase manganese profiles (figure 4) and particle transport rates within the same intervals (Aller 1980; Sundby & Silverberg 1984). Define $\hat{C}_{Mn}$ as the solid phase reactive manganese concentration, mass/volume total sediment; z as the depth coordinate, origin at interface, positive into sediment; t as time; D_B as the particle mixing coefficient; and $\hat{R}_{Mn}$ as the solid manganese net reduction rate. Then at steady state, no compaction:

$$\partial \hat{C}_{Mn}/\partial t = 0 = D_B \partial^2 \hat{C}_{Mn}/\partial z^2 - \hat{R}_{Mn}(z). \tag{1}$$

Because only the upper *ca.* 5 cm are considered, for the present purposes D_B is assumed constant (figure 2). The distributions of reactive $\hat{C}_{Mn}$, defined by subtracting the apparent asymptotic value of manganese at depth (*ca.* 5 cm) from overlying values, are given approximately by simple exponential functions in most of the measured cases. This gives

$$R(z) \approx D_B \beta^2 \hat{C}_{T,Mn}\, e^{-\beta z}, \tag{2}$$

where $\hat{C}_{T,Mn}$ is the solid reactive manganese at z equal to zero, and β is the attenuation constant.

The manganese reduction flux supported by these rates below the oxygenated zone is given roughly by the integral of equation (2) (the reaction rate) from 1 cm (near base of O_2 penetration) to 4 cm depth (approximate base of substantial excess manganese penetration). Calculations made from total manganese distributions in two cores ($\hat{C}_{T,Mn} = 4.6$ and 4.5 μmol cm^{-3}; $\beta = 0.68$ and 0.59 cm) and the leachable manganese profile determined by Balistrieri & Murray (1986) ($\hat{C}_{T,Mn} = 1.5$, $\beta = 0.81$) result in an average flux of $(76 \pm 28)\, D_B$ μmol cm^{-2} a^{-1} where D_B is in units of cm^2 a^{-1}. Assuming initial manganese oxide and organic carbon oxidation states of +4 and 0 respectively, the quantity of carbon reductant required to support the manganese gradient is $(38 \pm 13) D_B$ μmol cm^{-2} a^{-1}.

This implies that the entire average annual input of organic carbon, as measured by sediment traps, could be oxidized by manganese at values of $D_B > 1$ cm^2 a^{-1}. The measured range of D_B in the upper few centimetres is greater than, or equal to 10 cm^2 a^{-1} indicating a substantial mismatch between apparent carbon supply and estimated manganese reduction rates. These discrepancies could arise because of a combination of factors including overestimates of D_B, underestimates of organic carbon flux, or because of non-steady-state supply of carbon reductant in pulses and associated pulsed biological activity. Although estimates of D_B from ^{234}Th excess distributions in surface sediments may be maxima because of interface disturbance, the ^{210}Pb excess profiles indicate that mixing rates in the upper 5–8 cm are at least 5–10 times the rate of *ca.* 1 cm^2 a^{-1} in underlying sediment (figure 2). The supply of carbon measured by sediment traps is also known to vary by 5–10 times seasonally (Honjo 1982). It is possible that the solid phase distributions represent partly relict profiles from such periods of greater carbon supply. A variety of *ad hoc* combinations of measurement errors and non-steady-state processes can be invoked to explain discrepancies. Regardless of these, the major conclusion must be that manganese reduction can account for the oxidation of the entire organic carbon supply or at least major portion of the supply in this area.

A single *in situ* benthic chamber estimate of Mn^{2+} flux (*ca.* 2 nmol cm^{-2} d^{-1}; Aller *et al.* 1987) and numerous pore water profiles indicate that only a small fraction of the Mn^{2+} produced is released into overlying water. This means that the manganese cycle is essentially internal in these deposits and that much of the O_2 flux to the sediment (*ca.* 230 ± 65 nmol cm^{-2} d^{-1} from O_2 microelectrode profiles) must be consumed by the reoxidation of Mn^{2+} rather than directly by organic carbon during aerobic respiration.

Particle reworking, redox reaction balances and reaction rates

It can be readily shown that particle reworking during bioturbation has a critical role in determining the relative balance between aerobic and anaerobic decomposition pathways and, in particular, the importance and rate of manganese cycling. This is done here by use of a unified series of simple transport-reaction models for organic carbon, oxygen, nitrate, and manganese solid and solute distributions. It is assumed that during the initial stages of decomposition at least, the oxidation rate of reactive organic fractions is largely independent of oxidant (Westrich 1983). The major variables and driving forces in these models are therefore the supply, reactivity and distribution of metabolizable organic carbon, that is, reductant.

The decomposition of organic matter is phenomenologically well-described by first-order reaction kinetics in which the rate is simply proportional, through a rate constant $\hat{k}_c$, to the

quantity of reactant (Skopensev 1981; Berner 1980). The average value of $\hat{k}_c$ is not strictly constant with time and varies as the relative abundance of different fractions of organic matter change (Jorgensen 1977; Westrich & Berner 1984; Middlebury 1989). Nevertheless, over relatively restricted intervals of time, or depth intervals of sediment, a single value of $\hat{k}_c$ is a good approximation and describes the basic decomposition behaviour well (Berner 1980).

It is further assumed here that biological mixing at constant D_B dominates particle transport over the sediment interval of interest, the flux of reactive organic carbon, $\hat{J}_c$, to the sediment–water interface is constant, and that reactive carbon is eventually used up at depth. The vertical distribution of reactive carbon at steady state is given by:

$$\partial \hat{C}_c/\partial t = 0 = D_B \partial^2 \hat{C}_c/\partial z^2 - \hat{k}_c \hat{C}_c, \tag{3a}$$

$$z = 0, \quad D_B \partial \hat{C}_c/\partial z = -\hat{J}_c, \tag{3b}$$

$$z \to \infty; \quad \hat{C}_c \to 0, \tag{3c}$$

so that

$$\hat{C}_c = [\hat{J}_c/(\alpha D_B)]\, e^{-\alpha z}, \quad \alpha = \hat{k}_c/D_B, \tag{4a, b}$$

$$\hat{R}_c = d\hat{C}_c/dt = \alpha \hat{J}_c\, e^{-\alpha z}, \quad R_c = \hat{R}_c/\Phi, \tag{5a, b}$$

where Φ is porosity, $\hat{R}_c$ is the rate of carbon decomposition (mass/volume total sediment), R_c is the rate of carbon decomposition (mass/volume pore water).

This basic model, with varied boundary conditions, has been used by numerous investigators (Berner 1980; Aller 1982; Grundmanis & Murray 1982; Emerson *et al.* 1985).

The corresponding reaction rates for O_2, NO_3^-, and Mn reduction by carbon are derived from the stoichiometric relations of table 1, equation (5), the assumption of oxidant independent rates of carbon oxidation and, in the case of simultaneous NO_3^- and Mn reduction, an assumed branch ratio between reactions:

$$R_{O_2,c} = \gamma_{O_2} R_c, \tag{6a}$$

$$R_{dN} = \gamma_{dN} F_{dN} R_c, \tag{6b}$$

$$R_{Mn} = \gamma_{Mn} F_{Mn} R_c, \tag{6c}$$

where $R_{O_2,c}, R_{dN}, R_{Mn}$ are the rates of O_2, NO_3^- and manganese reduction by carbon (mass/volume pore water), $\gamma_{O_2}, \gamma_{dN}, \gamma_{Mn}$ are the stoichiometric mole ratios of O_2, NO_3^- and manganese reduction to direct organic carbon oxidation, and F_{Mn}, F_{dN} are reaction branch ratios for Mn and NO_3^- reduction ($F_{Mn} = 1 - F_{dN}$).

The definition of γ_{O_2} differs from common usage for reasons that will become clear. In the present case, nitrification is not implicitly included so that, in general, $\gamma_{O_2} = 1$ if the carbon oxidation state is 0. The value of γ_{dN} is taken as that for denitrification, $\frac{4}{5}$, where the reaction product is N_2. γ_{Mn} is approximately 2 (table 1) (Murray *et al.* 1984).

In a similar way the rate of NH_4^+ production, R_N, is

$$R_N = \gamma_N R_c, \tag{6d}$$

where γ_N is the nitrogen:carbon stoichiometric release ratio.

These reactions occur in the relative stratigraphy depicted in figure 5. O_2 is absent below $z = L_{O_2}$, NO_3^- is depleted by $z = L_N$, and Mn^{2+} reaches saturation with respect to a reduced solid such as carbonate at L_{Mn}. Oxidation of NH_3 (nitrification) and manganese is assumed to occur

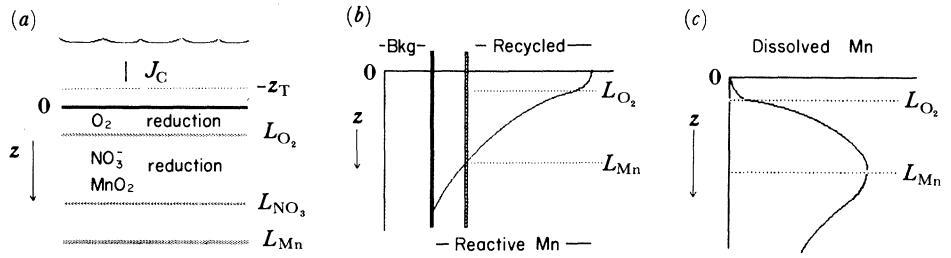

FIGURE 5. (*a*) General, vertically averaged diagenetic zones and relative relations of depth boundaries $-z_T$, L_{O_2}, L_N, L_{Mn} used in modelling. (*b*) Relation of recycled solid manganese to total manganese. (*c*) Pore water Mn features envisioned for model distributions.

above L_{O_2}. To this point, the conceptual bases for reactions in the model are comparable with many models of decomposition oxidation–reduction and hydrolysis reactions (see, for example, Berner 1980; Bender & Heggie 1984; Emerson *et al.* 1985).

A fundamental premise of previous models of this type used in the deep sea is that no significant reactive organic carbon escapes the zone where O_2 is present. This assumption is made either explicitly (Emerson *et al.* 1985) or implicitly by assuming fixed stoichiometric factors such as the nitrogen:carbon Redfield ratio for reactions such as nitrification in the oxygenated zone (Jahnke *et al.* 1982; Goloway & Bender 1982; Bender & Heggie 1984). In the latter cases, in effect, diffusible reduced species such as NH_4^+ produced below the zone of oxygenation are not allowed to reoxidize. Although appropriate for pelagic sediments when carbon is limiting, these assumptions are not necessarily valid for organic-rich hemipelagic sediments with active benthic communities. A critical calculation is how much reactive carbon initially escapes aerobic metabolism and thus can supply reduced species other than carbon capable of reducing O_2. The oxidation of these reduced species further biases decomposition processes toward less aerobic metabolism, allowing greater carbon escape from the oxygenated zone. The eventual balance between aerobic and anerobic metabolism is very different from when reoxidation is not considered.

In the present case the major diffusible reduced species capable of competing with carbon for O_2 are NH_4^+ and Mn^{2+}. Because there are no significant net precipitation reactions for NH_4^+ in normal marine sediments, at steady state the average rate of nitrification, $R_{N,ox}$ in the oxygenated zone is:

$$R_{N,ox} = \frac{f_N}{L_{O_2}} \int_0^\infty R_N \, dz, \tag{7}$$

where f_N is the fraction of total NH_4^+ produced in sediment escaping into overlying water. The corresponding flux of O_2 necessary to sustain this rate of nitrification is $2R_{N,ox} L_{O_2}$.

Assuming that pore water Mn^{2+} attains a maximum concentration at depth L_{Mn}, where saturation is reached, then the flux of O_2 necessary to oxidize the Mn^{2+} diffusing into the oxygenated zone to MnO_2 is

$$\tfrac{1}{2} f_{Mn} \int_{L_{O_2}}^{L_{Mn}} R_{Mn} \, dz, \tag{8}$$

where f_{Mn} is the fraction of upward diffusing Mn^{2+} that is oxidized. Given these definitions the total flux of O_2, J_{O_2}, into the sediment is

$$J_{O_2} = \int_0^{L_{O_2}} R_{O_2,c} \, dz + \tfrac{1}{2} f_{Mn} \int_{L_{O_2}}^{L_{Mn}} R_{Mn} \, dz + 2 f_N \int_0^\infty R_N \, dz. \tag{9}$$

PHILOSOPHICAL TRANSACTIONS OF THE ROYAL SOCIETY A MATHEMATICAL, PHYSICAL & ENGINEERING SCIENCES

The fraction, F_{O_2}, of the O_2 flux that directly oxidizes carbon is therefore

$$F_{O_2} = \left(\int_0^{L_{O_2}} R_{O_2,c}\, dz \right) \Big/ J_{O_2}. \tag{10}$$

This defines an apparent O_2/carbon stoichiometric factor, $1/F_{O_2}$, for O_2 uptake relative to CO_2 production from aerobic respiration. If Mn^{2+} oxidation and diffusion of NH_4^+ from below L_{O_2} are ignored, $F_{O_2} = 0.77$ and $1/F_{O_2} = 1.3$, assuming γ_N is taken as the Redfield ratio. This is the case considered in previous nitrification–denitrification models (Jahnke *et al.* 1982; Goloway & Bender 1982; Christensen & Rowe 1984). A comparable O_2 balance approach (equation (10)) has been used successfully by Mackin & Swider (1989) in nearshore sediments to examine the effect of sulphide oxidation and nitrification on aerobic–anaerobic reaction balances.

The total reaction rate of O_2 in the oxygenated zone, ignoring small-scale depth dependence in F_{O_2}, is now

$$R_{O_2} = R_c/F_{O_2}. \tag{11}$$

Application of these definitions allow a complete model for O_2 distribution to be calculated for various carbon fluxes ($\hat{J}_c$), reactivity ($\hat{k}_c$), and particle mixing rates (D_B). The value of F_{O_2} must be determined by iterative calculation to determine L_{O_2} and the proportion of reactive carbon escaping aerobic decomposition (Mackin & Swider 1989). To do this, it is necessary to simultaneously model components such as nitrogen and manganese subject to reoxidation. The basic models for O_2, NO_3^- and manganese are now outlined separately and then combined to explicitly illustrate the role of particle reworking in aerobic–anaerobic balances, and especially manganese cycling.

In each case, the rate of reduction of O_2, NO_3^- and manganese is assumed to be simply proportional to the organic carbon decomposition rate, that is, zero order in oxidant and first order in reductant concentration. If an oxidant (O_2, NO_3^-) is completely consumed within a modelled interval, both the concentration and flux of the oxidant must become zero at a specific depth. This depth is determined by iterative calculation. Use of these boundary conditions results in an analytical mathematical mimic to the more complex Michaelis–Menten uptake kinetics for calculating the distribution of a pore water oxidant, while allowing organic carbon to decompose at first-order rates (Boudreau & Westrich 1985). All model equations assume steady state and no compaction. The specific rate functions are given by equations (6)–(11).

Oxygen

Zone 0 (overlying water diffusive boundary layer; $-z_T \leqslant z \leqslant 0$):

$$\partial C_{O_2}/\partial t = 0 = D^\circ_{O_2} \partial C_{O_2}/\partial z, \tag{12a}$$

$$z = -z_T, \quad C_{0,O_2} = C_{T,O_2}, \tag{12b}$$

$$z = 0 \quad \text{when} \quad C_{0,O_2} = C_{1,O_2}, \tag{12c}$$

$$D^\circ_{O_2} \partial C_{0,O_2}/\partial z = \Phi D_{s,O_2} \partial C_{1,O_2}/\partial z. \tag{12d}$$

PHILOSOPHICAL TRANSACTIONS OF THE ROYAL SOCIETY A MATHEMATICAL, PHYSICAL & ENGINEERING SCIENCES

Zone 1 (oxygenated sediment layer, $0 \leqslant z \leqslant L_{O_2}$):

$$\partial C_{1,O_2}/\partial t = 0 = D_{s,O_2}\partial^2 C_{1,O_2}/\partial z^2 - R_{O_2}, \tag{13a}$$

$$z = 0 \quad \text{(as for zone 0)}, \tag{13b}$$

$$z = L_{O_2}, \quad C_{1,O_2} = 0, \tag{13c, d}$$

$$\partial C_{1,O_2}/\partial z = 0, \tag{13e}$$

where C_{0,O_2}; C_{1,O_2} are the concentrations of dissolved O_2 in zone 0 and zone 1, $-z_T$ is the top of the diffusive sublayer, $D^\circ_{O_2}, D_{s,O_2}$ are the free solution and whole sediment O_2 diffusion coefficients, L_{O_2} is the depth of oxygenated layer, and R_{O_2} is the O_2 reaction rate defined in equations (10) and (11).

Nitrate

The presence of a diffusive boundary layer is not explicitly considered for NO_3^- but is implicit through the calculation of L_{O_2}.

Zone 1 (nitrification, oxygenated sediment layer; $0 \leqslant z \leqslant L_{O_2}$):

$$\partial C_{1,NO}/\partial t = 0 = D_{s,NO}\partial^2 C_{1,NO}/\partial z^2 + R_{N,ox}, \tag{14a}$$

$$z = 0 \quad \text{when} \quad C_{1,NO} = C_{T,NO}, \tag{14b}$$

$$z = L_{O_2} \quad \text{when} \quad C_{1,NO} = C_{2,NO}, \tag{14c}$$

$$\partial C_{1,NO}/\partial z = \partial C_{2,NO}/\partial z. \tag{14d}$$

Zone 2 (denitrification; $L_{O_2} \leqslant z \leqslant L_N$):

$$\partial C_{2,NO}/\partial t = 0 = D_{s,NO}\partial^2 C_{2,NO}/\partial z^2 - R_{dN}, \tag{15a}$$

$$z = L_{O_2}, \quad \text{as in (14c, d)}, \tag{15b, c}$$

$$z = L_N \quad \text{when} \quad C_{2,NO} = 0, \tag{15d}$$

$$\partial C_{2,NO}/\partial z = 0, \tag{15e}$$

where $C_{1,NO}, C_{2,NO}$ are the concentrations of NO_3^- in zone 1 and 2, $D_{s,NO}$ is the whole sediment diffusion coefficient, L_N is the lower depth limit of denitrification, and $R_{N,ox}, R_{dN}$ and the reaction rates as in equations (6*b*) and (7).

Manganese, solid

All previously reported models of sedimentary manganese distributions have assumed that Mn^{2+} oxidation–precipitation is a first-order reaction proportional to dissolved Mn^{2+} concentration (Burdige & Gieskes 1983; Taylor 1986). Taylor (1986) experimentally demonstrated that except at extremely low O_2 of a few μM, sedimentary manganese oxidation in organic-rich nearshore sediments is essentially independent of O_2. He found that Mn^{2+} oxidation was simply proportional to solid phase manganese, although probably for reasons related phenomenologically to microbiological activity rather than solid phase autocatalysis as such. In the following formulations, Mn^{2+} oxidation is assumed to be first order with respect to solid phase recycled manganese. This assumption results in a more realistic correspondence

between shapes of calculated and observed distributions but regardless of which of these kinetic formulations is used no major conclusions made subsequently are changed.

The model developed here also considers only that portion of the diagenetically reactive manganese that is recycled between oxic and anoxic regions of the deposit (figure 5). For the present purposes it is assumed that once saturation with respect to a reduced phase is reached at a depth L_{Mn}, upward recycling of manganese ceases. This is not strictly correct in bioturbated deposits but is used here as an approximation. The mass flux of recycled manganese is also assumed to dominate any flux of manganese from the overlying water so that the downward flux at $z = 0$ can be taken as vanishingly small. The equations are:

zone 1 (oxidation–precipitation; $0 \leqslant z \leqslant L_{\mathrm{O_2}}$);

$$\partial \hat{C}_{1,\mathrm{Mn}}/\partial t = 0 = D_{\mathrm{B}}\,\partial^2 \hat{C}_{1,\mathrm{Mn}}/\partial z^2 + \hat{k}_{\mathrm{ox}}\,\hat{C}_{1,\mathrm{Mn}}, \tag{16a}$$

$$z = 0, \partial \hat{C}_{1,\mathrm{Mn}}/\partial z = 0, \tag{16b}$$

$$z = L_{\mathrm{O_2}} \quad \text{when} \quad \hat{C}_{1,\mathrm{Mn}} = \hat{C}_{2,\mathrm{Mn}}, \tag{16c}$$

$$\partial \hat{C}_{1,\mathrm{Mn}}/\partial z = \partial \hat{C}_{2,\mathrm{Mn}}/\partial z \tag{16d}$$

zone 2 (reduction–dissolution; $L_{\mathrm{O_2}} \leqslant z \leqslant L_{\mathrm{Mn}}$):

$$\partial \hat{C}_{2,\mathrm{Mn}}/\partial t = 0 = D_{\mathrm{B}}\,\partial^2 \hat{C}_{2,\mathrm{Mn}}/\partial z^2 - \hat{R}_{\mathrm{Mn}}, \tag{17a}$$

$$z = L_{\mathrm{O_2}}, \quad \text{as (16}c, d\text{)}, \tag{17b}$$

$$z = L_{\mathrm{Mn}} \quad \text{when} \quad \hat{C}_{2,\mathrm{Mn}} = 0, \tag{17d}$$

where $\hat{C}_{1,\mathrm{Mn}}$, $\hat{C}_{2,\mathrm{Mn}}$ are the solid phase manganese concentrations in zone 1 and 2 (mass/total sediment volume), $\hat{k}_{\mathrm{ox}}$ is the first-order oxic precipitation rate constant, L_{Mn} is the depth of pore water $\mathrm{Mn^{2+}}$ maximum (solute gradient = 0) and $\hat{R}_{\mathrm{Mn}}$ is equal to R_{Mn}/Φ, equation (6c). The value of $\hat{k}_{\mathrm{ox}}$ is determined from the pore water $\mathrm{Mn^{2+}}$ distribution based on the depth $L_{\mathrm{O_2}}$ and the flux of $\mathrm{Mn^{2+}}$ across the sediment–water interface, $z = 0$.

Manganese, dissolved

Three to four dissolved manganese reaction zones are often assumed (Klinkhammer 1980; Burdige & Gieskes 1983; Taylor 1986). An upper zone of either no reaction or oxic equilibrium; a zone of net oxidation–precipitation of upward diffusing manganese; a zone of net production; and a zone of net anoxic precipitation. In the present case of organic-rich sediments the uppermost zone of oxic equilibrium is extremely small and is ignored or assumed to have the overlying water concentration, and the lower zone of equilibrium is not explicitly modelled. A simple two reaction zone model is assumed with oxidation–precipitation in the upper zone and production in the lower.

The base of the lower zone (L_{Mn}) is defined by equilibrium saturation and concentration control by an anoxic phase such as manganese carbonate.

Zone 1 (oxidation–precipitation; $0 \leqslant z \leqslant L_{\mathrm{O_2}}$):

$$\partial \hat{C}_{1,\mathrm{Mn}}/\partial t = 0 = D_{\mathrm{s,Mn}}\,\partial^2 C_{1,\mathrm{Mn}}/\partial z^2 - \hat{k}_{\mathrm{ox}}\,\hat{C}/\Phi, \tag{18a}$$

$$z = 0 \quad \text{when} \quad C_{1,\mathrm{Mn}} = 0, \quad \partial C_{1,\mathrm{Mn}}/\partial z = 0, \tag{18b, c}$$

$$z = L_{\mathrm{O_2}} \quad \text{when} \quad C_{1,\mathrm{Mn}} = C_{2,\mathrm{Mn}}, \quad \partial C_{1,\mathrm{Mn}}/\partial z = \partial C_{2,\mathrm{Mn}}/\partial z. \tag{18d, e}$$

PHILOSOPHICAL TRANSACTIONS OF THE ROYAL SOCIETY A MATHEMATICAL, PHYSICAL & ENGINEERING SCIENCES

Zone 2 (production; $L_{O_2} \leqslant z \leqslant L_{Mn}$):

$$\partial C_{2,Mn}/\partial t = 0 = D_{s,Mn}\,\partial^2 C_{2,Mn}/\partial z^2 + R_{Mn}, \tag{19a}$$

$$z = L_{O_2}, \quad \text{as } (18d, e), \tag{19b, c}$$

$$z = L_{Mn} \quad \text{when} \quad \partial C_{2,Mn}/\partial z = 0, \tag{19d}$$

where $C_{1,Mn}$ is the dissolved manganese concentration in zone 1 and 2, $D_{s,Mn}$ is the whole sediment Mn^{2+} diffusion coefficient, R_{Mn} is the Mn^{2+} production rate and L_{Mn} is the depth of maximum Mn^{2+} concentration; saturation.

The conditions (18*b*, *c*) can be assigned to any depth $0 \leqslant z < L_{O_2}$. This focuses all manganese precipitation into the resulting sediment interval. For the present demonstration, the interval is taken as the entire oxygenated layer. The value of $\hat{k}_{ox}$ is determined by the mass balance between the steady-state flux from the underlying production zone and the necessity to precipitate that flux into the defined sediment interval.

The general solutions to the various model equations are given in Appendix 1.

Evaluation of model distributions

Model distributions are determined by successive evaluation and iteration to find L_{O_2} and F_{O_2}. The carbon flux $\hat{J}_c$, reactivity $\hat{k}_c$ and particle mixing rate D_B, define the carbon penetration pattern. An initial estimate of the O_2 distribution is calculated (equations (12) and (13)). This step is essentially the model of Emerson *et al.* (1985). The proportion of the carbon surviving the oxygenated zone (L_{O_2}) is determined and the resulting production of Mn^{2+} calculated. The upward diffusing Mn^{2+} and NH_4^+ are oxidized at an efficiency given by the fractions f_N, f_{Mn}, which define the tendency for escape of reduced species into overlying water. These are taken as 1 in all calculations. In the present model evaluation the decomposition branch ratios, F_N and F_{Mn}, were taken as 0.3 and 0.7 respectively. This generally results in NO_3^- depletion between 5–10 cm for the cases considered. The depth L_{Mn} is also set to 10 cm (observed value). After calculation of the quantity of upward diffusing Mn^{2+} and NH_4^+, which are reoxidized, the calculations of F_{O_2} and L_{O_2} are repeated and the carbon escape from the aerobic zone re-estimated. The iterations are repeated in practice until the 'limiting' values of F_{O_2} and L_{O_2} are within less than 1% of a previous calculation. Whole sediment diffusion coefficients were estimated from the relation $D_s \approx \Phi^2 D°$, where $D°$ is the appropriate free solution diffusion coefficient at 2 °C (Li & Gregory 1974; Ferrell & Himmelblau 1967) and the porosity, $\Phi = 0.85$ (Ullman & Aller, 1982). Values for C_T are 110, 41.5, and 0 μM for O_2, NO_3^-, and Mn^{2+} respectively, unless otherwise indicated.

The values of F_{O_2} (ratio of O_2 flux oxidizing carbon to total O_2 flux) and the proportion of aerobic carbon oxidation are strong functions of D_B, $\hat{k}_c$ and C_{T,O_2} for a given carbon flux (figure 6). In the general range of reactivity ($\hat{k}_c \approx 0.7\ a^{-1}$) and bottom O_2 ($\approx 110\,\mu M$) expected for the PB site, biogenic particle reworking as represented by D_B must have a major influence on the relative proportion of aerobic to anaerobic decomposition of organic carbon. The total flux of O_2 to the bottom is not greatly changed by variations in D_B (figure 7) because the net burial, or loss (N_2), of reduced compounds is kept small in these considerations ($L_{Mn} = 10$ cm is large relative to $(\hat{k}_c/D_B)^{\frac{1}{2}}$).

Solid phase and pore water manganese model profiles corresponding to different rates of mixing ($\hat{J}_c$, $\hat{k}_c$ fixed) demonstrate the expected response of manganese to biogenic reworking

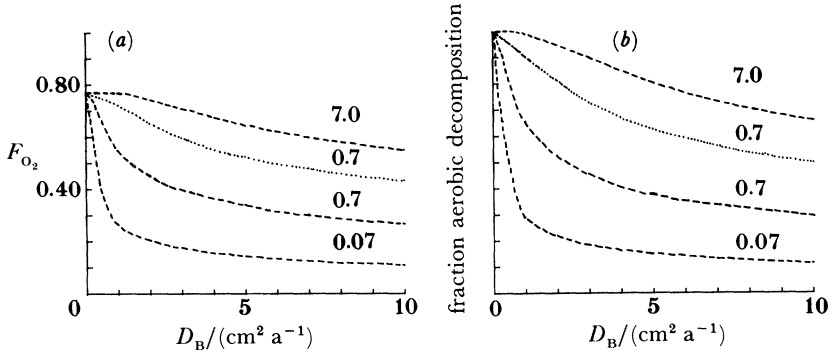

FIGURE 6. (*a*) The apparent stoichiometric ratio F_{O_2} and (*b*) fraction of aerobic decomposition relative to total carbon is a strong function of mixing in the range of carbon activity, $\hat{k}_c$, typical of fresh organic matter (*ca.* 0.7 a^{-1}). $\hat{J}_c = 40$ μmol cm^{-2} a^{-1}, the sediment trap measured annual mean flux is used in all cases. The numbers above the lines in each graph give the value of $\hat{k}_c$.

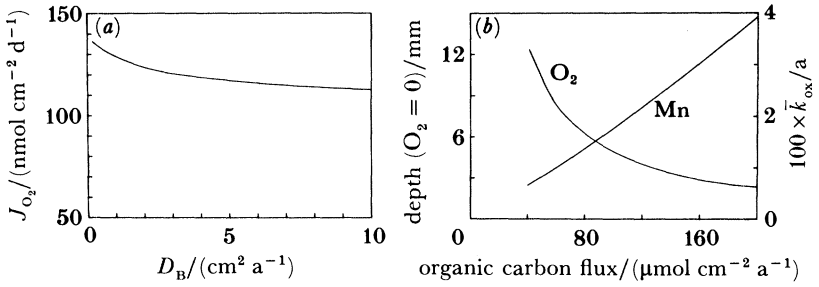

FIGURE 7. The total flux of O_2 (not including macrofaunal respiration) is largely independent of D_B when little storage or loss of reduced products occurs (L_{Mn} large). The decrease that occurs is due to increased loss of precipitated Mn^{2+} (e.g. $MnCa(CO_3)_2$) and N_2. (*a*) L_{O_2} ranges from 1.29 to 1.55 cm in this case where $\hat{J}_c = 40$ μmol cm^{-2} d^{-1}, $\hat{k}_c = 0.7$ a^{-1}. (*b*) Both L_{O_2} and $\hat{k}_{ox}$ (Mn^{2+} oxidation rate) are strong functions of $\hat{J}_c$ at fixed D_B (= 10 cm^2 a^{-1} in this example) and $\hat{k}_c$ (= 0.7 a^{-1}).

without irrigation (figure 8). Surface enrichment of solid manganese decreases and pore water manganese at depth increases as particle mixing (D_B) increases (see also Taylor 1986). If the observed magnitudes of solid phase manganese enrichments at PB are steady state, either the carbon flux is considerably higher than the *ca.* 40 μmol cm^{-2} a^{-1} average assumed here (figures 7 and 9) or D_B is about 10 times slower than the various measures of particle reworking indicate. This corroborates the simple calculation made previously. A lower carbon reactivity ($\hat{k}_c$) would also increase surface enrichment to a degree but substantially lower $\hat{k}_c$ results in decreases in manganese enrichments. The measured O_2 penetration and diffusive flux estimates are also more closely approximated by a $\hat{J}_c$ 2–3 times the sediment trap value (figure 7).

The cycling of manganese is greatly intensified by particle reworking (Aller 1980; Sundby & Silverberg 1984). Although surface manganese enrichments are less accentuated at high D_B, the turnover of manganese in both the oxic and anoxic zones greatly increases as D_B increases (figure 10). This conclusion depends, as do the profiles, on f_{Mn} (fraction Mn^{2+} oxidized in oxygenated zone) remaining constant, or equivalently, microbial oxidation increasing to accommodate increased Mn^{2+} supply. Rapid turnover must promote scavenging at the sediment–water interface through maintenance of 'fresh' manganese oxide surfaces (see, for example, Balistrieri & Murray 1986). In sulphidic sediments, biogenic reworking presumably also enhances a lithotrophic (sulphur-based) pathway of manganese-reduction and anaerobic

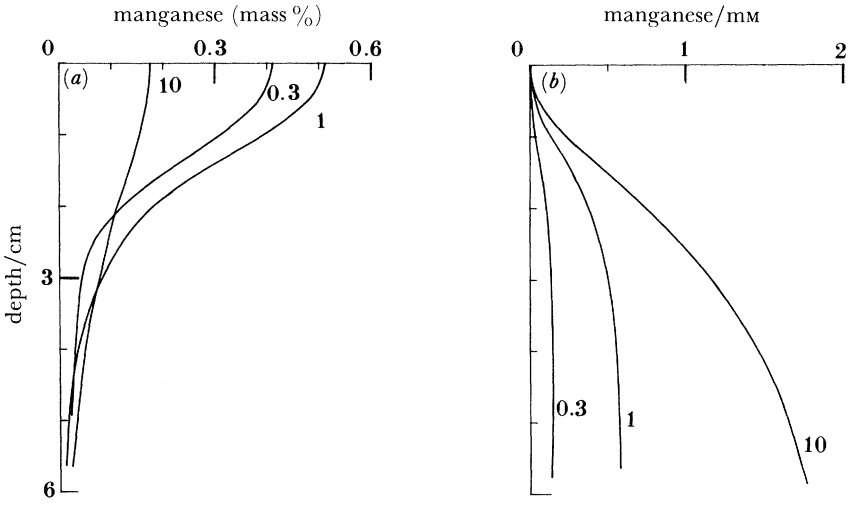

FIGURE 8. Model profiles of (*a*) solid phase and (*b*) pore water manganese at variable D_B (0.3–10 cm^2 a^{-1}). ($\hat{J}_c = 40$ μmol cm^{-2} a^{-1}; $\hat{k}_c = 0.7$ a^{-1}.)

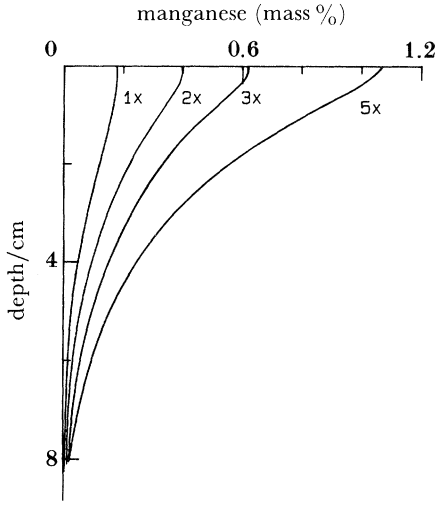

FIGURE 9. Recycled manganese increases with carbon flux. $\hat{J}_c$. The curves shown are for 1, 2, 3, and 5 times the reported yearly average of *ca.* 40 μmol cm^{-2} a^{-1} with $D_B = 10$ cm^2 a^{-1} and $\hat{k}_c = 0.7$ a^{-1}.

sulphur-oxidation by increasing contact between manganese oxides and iron sulphides (Aller & Rude 1988).

The concentration ranges of Mn^{2+} in model pore water profiles are higher than observed (figures 3 and 8). This implies, assuming the basic premises of the model are otherwise correct, than either irrigation or anoxic precipitation, or both, are substantial in the upper decimeter of sediment. The net extraction of Mn^{2+} due to diffusion into burrows can be mimicked mathematically by a 'non-local' source–sink exchange process proportional to concentration differences between burrow or tube water and surrounding pore waters (Kipphut & Martens 1983; Emerson *et al.* 1984). For a variation in carbon flux of 1–5 times the yearly average, an exchange constant, $\eta \approx 0.08$–0.013 d^{-1}, is required to lower the highest model pore water concentrations ($D_B = 10$ cm^2 a^{-1}) to the observed range of 200–400 μM. This could be accomplished by just a few hundred per m^2 actively irrigated burrows in the burrow diameter

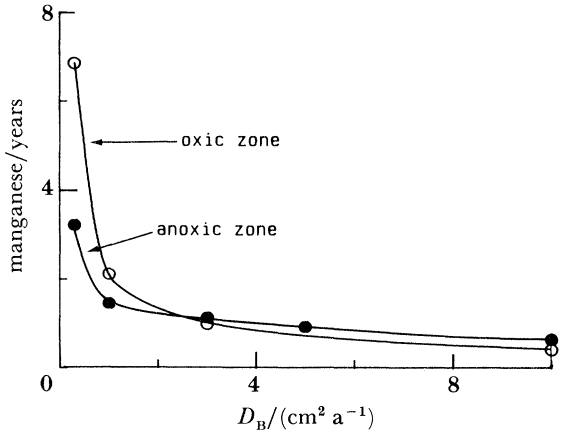

FIGURE 10. The calculated turnover (residence) time in years of the recycled manganese inventory in the oxic and anoxic (suboxic) zones are variable D_B ($\hat{J}_c = 40$ μmol cm^{-2} a^{-1}; $\hat{k}_c = 0.7$ a^{-1}).

size range 0.1–1 cm as estimated by a radial diffusion model (Aller & Yingst 1985). Because the Mn^{2+} diffusing toward burrows may be precipitated completely or in part around burrows; the impact of irrigation on bulk (average) solid phase manganese distributions cannot be readily evaluated at this time. Depending on the proportion of Mn^{2+} escaping into overlying water, Mn^{2+} diffusing towards burrows may or may not appear as recycled manganese at the sediment–water interface. Irrigation and oxidation of reduced metabolites at depth also decreases reoxidation by vertical diffusive flux and thereby indirectly increases O_2 penetration at the upper sediment–water interface. Because only *ca.* 5–10% of the total Mn^{2+} production is likely to be lost from solution or the sediment through irrigation, for the range of $\hat{J}_c$, $\hat{k}_c$, D_B, C_{T,O_2}, considered here, the relative aerobic–anaerobic reaction balances are not substantially altered.

It can be shown using a radial geometry diffusion–reaction model similar to equations (17) and (18) that a higher proportion of the flux of Mn^{2+} into the oxidized zone is precipitated for a given $\hat{k}_{ox}$ and oxidized zone thickness in a radical compared to a planar geometry. This does not preclude escape of Mn^{2+} into the burrow centre but does bias the distributions toward greater percentage capture of Mn^{2+} in a radial relative to planar geometry for a given exposed-surface : bulk-volume ratio of the oxidized zone.

The depletion of metabolites and potential coprecipitants such as HCO_3^- from pore water during irrigation can stimulate Mn^{2+} production rates and decomposition in nearshore organic-rich sediments, and presumably in comparably reactive deep-sea deposits such as in the Panama Basin (figure 11). In effect this causes $\hat{k}_c$ to vary as a function of burrow density and further increases reaction rate heterogeneity in bioturbated deposits. The coupling between macrofaunal activities and manganese cycling can therefore be further intensified by irrigation and burrow construction activity.

These various observations, models and calculations demonstrate some of the ways decomposition reaction balances and rates, particularly manganese cycling, are influenced by macrobenthic activities in surface sediments. Qualitative indications of these interactions and apparent adaptation of infauna to promoting manganese cycling in the Panama Basin, are also given by common biogenic structures found in these deposits (X-radiograph not shown for lack of space). Manganese oxide tubes composing the central axes of spiral burrow structures are

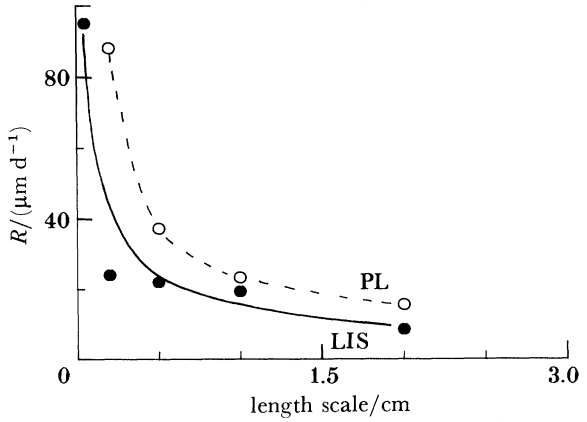

FIGURE 11. Irrigation results in depletion of metabolites and reactants from sediment, presumably stimulating production of Mn^{2+}. In these examples from nearshore muds (LIS = Long Island Sound, Connecticut; PL = Priest Landing, Georgia) Mn^{2+} production increases as the characteristic diffusion scale or thickness of otherwise identical sediment decreases in anoxic diffusion cell experiments (see Aller & Mackin 1989). This is comparable with decreasing spacing (sediment thickness) between burrows.

suggestive of close associations of macrofauna with both chemoautotrophic and heterotrophic microbial activity during manganese oxidation–reduction. Whether these represent microbial 'gardening' or 'farming' associations remains to be found out.

CONCLUSIONS

In organic-rich hemipelagic sediments, the decomposition of organic matter and diagenetic properties of deposits can be dominated by anaerobic metabolism, particularly suboxic reactions such as NO_3 and manganese reduction. The Panama Basin of the east equatorial Pacific is one such area where oceanographic upwelling and tectonic conditions result in sediments having both abundant reactive carbon and manganese. The activities of macroinfauna can dramatically alter oxic–suboxic reaction balances, and promote intense recycling of manganese in the bioturbated zone of these sediments. Manganese reduction is capable of oxidizing the entire estimated annual flux of carbon. Unified transport-reaction models of organic carbon, O_2, NO_3 and manganese which take into account reoxidation of reduced metabolites, demonstrate that direct decomposition of carbon by O_2 decreases dramatically as particle mixing increases during bioturbation. When little storage or escape from the sediment of reduced reaction products occurs, the O_2 flux to the sea floor is utilized largely in the reoxidation of anaerobic metabolites rather than aerobic respiration. Manganese cycles rapidly between oxidized and reduced zones in these cases as a function of particle reworking, carbon flux, carbon reactivity and overlying O_2 concentration. A major effect of reworking is to increase the proportion of anaerobic decomposition but to decrease storage of reduced reaction products and thus diagenetic evidence of reaction pathways. Irrigation depletes Mn^{2+}, increases Mn^{2+} production and creates radial diffusion reaction geometries at depth but probably does not substantially alter overall oxic–suboxic reaction balances in a deposit when decomposition rates decrease sharply below the sediment–water interface and benthic population abundances are moderate. Both quantitative models and qualitative observations, such as types of biogenic structures, indicate strong interactions between macrobenthos and manganese cycling in hemipelagic sediments of the east equatorial Pacific.

Work on the Panama Basin was made possible through collaborations at various times with J. E. Mackin, P. O. J. Hall, J. F. Grassle, R. B. Whitlatch, S. Honjo, D. J. DeMaster, P. D. Rude, J. K. Cochran, J. Cole and J. Y. Aller. Laboratory assistance came from S. Wirick, R. Nelson, M. Kino, S. Dougherty and others over the years. M. A. Lau aided in manuscript preparation. This work was supported by NSF OCE 86-13688 and predecessors.

Appendix 1

General solutions (equations (12) and (13)):

O_2 (zone 0)

$$C_{0,O_2} = A_0 z + B_0,$$

O_2 (zone 1)

$$C_{1,O_2} = B_1 + A_1 z + (\gamma_{O_2} \hat{J}_c e^{-\alpha z}/\Phi\alpha D_{s,O_2}),$$

L_{O_2} must satisfy

$$C_{T,O_2} = \frac{\gamma_{O_2}\hat{J}_c}{\Phi\alpha D_{s,O_2}}[1-(L_{O_2}\alpha+1)\,e^{-\alpha L_{O_2}}] + \frac{\gamma_{O_2}\hat{J}_c}{D^\circ}(1-e^{-\alpha L_{O_2}})\,z_T.$$

(Note that γ_{O_2} is replaced by $1/F_{O_2}$ when reoxidation of reduced metabolites takes place.)

General solutions (equations (14) and (15)):

NO_3 (zone 1)

$$C_{1,NO} = B_1 + A_1 z - R_{N,ox} z^2/2D_{s,N},$$

NO_3 (zone 2)

$$C_{2,NO} = B_2 + A_2 z + \gamma_{dN} F_{dN} \hat{J}_c e^{-\alpha z}/\Phi D_{s,N^a},$$

L_N must satisfy

$$C_{T,NO} = \frac{\gamma_{dN} F_{dN} \hat{J}_c}{\Phi D_{s,N^a}}[e^{-\alpha L_{O_2}}(1+\alpha L_{O_2}) - e^{-\alpha L_N}(1+\alpha L_N)] - \frac{R_{N,ox} L_{O_2}}{2D_{s,N}}.$$

General solutions (equations (16) and (17)):

Manganese, solid (zone 1)

$$\hat{C}_{1,Mn} = \hat{B}_1 \cos(\sigma z), \quad \sigma = \sqrt{(\hat{k}_{ox}/D_B)},$$

Manganese solid (zone 2)

$$\hat{C}_{2,Mn} = \hat{A}_2 z + \hat{B}_2 + (\gamma_{Mn} F_{Mn} \hat{J}_c e^{-\alpha z}/D_B\alpha).$$

Mn, dissolved ($L_1 = 0$) (zone 1)

$$C_{1,Mn} = A_1 z + B_1 - \hat{k}_{ox}\hat{B}_1 \cos(\sigma z)/\Phi\sigma^2 D_{2,Mn},$$

Mn, dissolved (zone 2)

$$C_{2,Mn} = A_2 z + B_2 - (\gamma_{Mn} F_{Mn} \hat{J}_c e^{-\alpha z}/\Phi\alpha D_{s,Mn}),$$

$\hat{k}_{ox}$ must satisfy

$$\hat{k}_{ox} = \gamma_{Mn} F_{Mn} \hat{J}_c (e^{-\alpha L_{O_2}} - e^{-\alpha L_{Mn}})\,\sigma/\hat{B}_1 \sin(\sigma L_{O_2}).$$

The constants A, B, $\hat{A}$, $\hat{B}$ are evaluated algebraically to satisfy the appropriate boundary conditions in each case. In the case of $\hat{C}_{1,Mn}$, an additional term, $\hat{A}_1 \sin(\sigma z)$, is required if precipitation is complete at a depth $z > 0$.

References

Aller, R. C. 1980 *Adv. Geophys.* **22**, 351–415.

Aller, R. C. 1982 The effects of macrobenthos on chemical properties of marine sediment and overlying water. In *Animal–sediment relations* (ed. P. L. McCall & M. J. Tevesz), pp. 53–102. New York: Plenum.

Aller, R. C. & DeMaster, D. J. 1984 *Earth planet. Sci. Lett.* **67**, 308–318.

Aller, R. C. & Yingst, J. Y. 1985 *J. Mar. Res.* **43**, 615–645.

Aller, R. C., Hall, P. O. J. & Rude, P. D. 1987 *Eos, Wash.* **68**, 1749.

Aller, R. C. & Mackin, J. E. 1989 *J. Mar. Res.* **47**, 411–440.

Balistrieri, L. S. & Murray, J. W. 1986 *Geochim. cosmochim. Acta* **48**, 921–929.

Bender, M. L. & Heggie, D. T. 1984 *Geochim. cosmochim. Acta* **48**, 977–986.

Bender, M. L., Jahnke, R., Weiss, R., Martin, W., Heggie, D. T., Orchardo, J. & Sowers, T. 1989 *Geochim. cosmochim Acta* **53**, 685–697.

Berner, R. A. 1980 *Early diagenesis*. Princeton University Press.

Bourdreau, B. P. & Westrich, J. T. 1984 *Geochim. cosmochim. Acta* **48**, 2503–2516.

Boström, K. & Petersen, M. 1969 *Mar. Geol.* **7**, 427–447.

Burdige, D. J. & Gieskes, J. M. 1983 *Am. J. Sci.* **283**, 29–47.

Chanton, J. P., Goldhaber, M. B. & Martens, C. S. 1987 *Geochim. cosmochim. Acta* **51**, 1187–1199.

Christensen, J. P. & Rowe, G. T. 1984 *J. Mar. Res.* **42**, 1099–1116.

Cole, J. J., Honjo, S. & Caraco, N. 1985 *Hydrobiologia* **122**, 193–197.

Cole, J. J., Honjo, S. & Erez, J. 1987 *Nature, Lond.* **327**, 703–704.

Emerson, S., Jahnke, R. & Heggie, D. 1984 *J. Mar. Res.* **42**, 709–730.

Emerson, S., Fischer, K., Reimers, C. & Heggie, D. 1985 *Deep Sea Res.* **32**, 1–21.

Ferrell, R. T. & Himmelblau, D. M. 1967 *J. chem. Engng. Data* **12**, 111–115.

Froelich, P. N., Klinkhammer, G. P., Bender, M. L., Luedtke, N. A., Heath, G. R., Cullen, D., Dauphin, P., Hammond, D., Hartman, B. & Maynard, V. 1979 *Geochim. cosmochim. Acta* **43**, 1975–1990.

Goloway, F. & Bender, M. 1982 *Limnol. Oceanogr.* **27**, 624–638.

Grundmanis, V. & Murray, J. W. 1982 *Geochim. cosmochim. Acta* **46**, 1101–1120.

Honjo, S. 1982 *Science, Wash.* **218**, 883.

Honjo, S., Spencer, D. W. & Farrington, J. W. 1982 *Science, Wash.* **216**, 516–518.

Jahnke, R. A., Emerson, S. R. & Murray, J. W. 1982 *Limnol. Oceanogr.* **27**, 610–623.

Jorgensen, B. B. 1979 *Limnol. Oceanogr.* **22**, 814–832.

Kipphut, G. W. & Martens, C. S. 1982 *Geochim. cosmochim. Acta* **46**, 2049–2060.

Klinkhammer, G. P. 1980 *Earth planet. Sci. Lett.* **49**, 81–101.

Laird, N. P. 1971. *J. Mar. Res.* **29**, 226–234.

Li, Y.-H. & Gregory, S. 1974 *Geochim. cosmochim. Acta* **38**, 703–714.

Lonsdale, P. F. 1976 *J. geophys. Res.* **81**, 1163–1176.

Love, C. M. & Aller, R. M. (eds) 1975 *EASTROPAC Atlas* V.10. U.S. Dept. Commerce Circ. (330 pages.)

Lyle M. 1983 *Limnol. Oceanogr.* **28**, 1026–1033.

Mackin, J. E. & Swider, K. T. 1989 *J. Mar. Res.* **47**, 681–716.

Manheim, F. T. & Lane-Bostwick, C. M. 1988 *Nature, Lond.* **335**, 59–61.

Middleburg, J. 1989 *Geochim. cosmochim. Acta*. (In the press.)

Moore, T. C., Heath, G. R. & Kowsmann, R. O. 1973 *J. Geol.* **81**, 458–472.

Murray, J. W., Balistrieri, L. S. & Paul, B. 1984 *Geochim. cosmochim. Acta* **48**, 1237–1247.

Pedersen, T. F. & Price, N. B. 1982 *Geochim. cosmochim. Acta* **46**, 59–68.

Reimers, C. E. 1987 *Deep Sea Res.* **34**, 2019–2035.

Skopintsev, B. A. 1981 Decomposition of organic matter of plankton, humification, and hydrolysis. In *Marine organic chemistry: evolution, composition, interactions and chemistry of organic matter in sea water* (ed. E. K. Duursma & R. Dawson), pp. 125–177. New York: Elsevier.

Spencer, D. W. 1979 *STIE cruise report.* R/V KNORR 73-17, July 25 to Aug. 8, Woods Hole, Massachusetts.

Sundby, B. & Silverberg, N. 1985 *Limnol. Oceanogr.* **30**, 372–381.

Taylor, R. J. 1986 Ph.D. thesis, Texas A&M University.

Ullman, W. J. & Aller, R. C. 1982 *Limnol. Oceanogr.* **27**, 552–556.

Westrich, J. T. 1983 Ph.D. thesis, Yale University.

Westrich, J. T. & Berner, R. A. 1984 *Limnol. Oceanogr.* **29**, 236–249.

PHILOSOPHICAL TRANSACTIONS OF THE ROYAL SOCIETY A MATHEMATICAL, PHYSICAL & ENGINEERING SCIENCES